Available online at www.sciencedirect.com
SCIENCE DIRECT®
Geomorphology 55 (2003) 363–380
GEOMORPHOLOGY
www.elsevier.com/locate/geomorph

High spatial resolution hyperspectral mapping of in-stream habitats, depths, and woody debris in mountain streams

W. Andrew Marcus[a,*], Carl J. Legleiter[b], Richard J. Aspinall[b], Joseph W. Boardman[c], Robert L. Crabtree[d]

[a] Department of Geography, University of Oregon, Eugene, OR 97403-1251, USA
[b] Department of Earth Sciences, Montana State University, Bozeman, MT 59717, USA
[c] Analytical Imaging and Geophysics, 4450 Arapahoe Ave, Suite 100, Boulder, CO 80303, USA
[d] Yellowstone Ecological Research Center, 7500 Jarmen Circle, Suite #2, Bozeman, MT 59715, USA

Received 29 January 2002; received in revised form 10 May 2002; accepted 10 March 2003

Abstract

This article evaluates the potential of 1-m resolution, 128-band hyperspectral imagery for mapping in-stream habitats, depths, and woody debris in third- to fifth-order streams in the northern Yellowstone region. Maximum likelihood supervised classification using principal component images provided overall classification accuracies for in-stream habitats (glides, riffles, pools, and eddy drop zones) ranging from 69% for third-order streams to 86% for fifth-order streams. This scale dependency of classification accuracy was probably driven by the greater proportion of transitional boundary areas in the smaller streams. Multiple regressions of measured depths (y) versus principal component scores ($x_1, x_2, \ldots, x_n$) generated R^2 values ranging from 67% for high-gradient riffles to 99% for glides in a fifth-order reach. R^2 values were lower in third-order reaches, ranging from 28% for runs and glides to 94% for pools. The less accurate depth estimates obtained for smaller streams probably resulted from the relative increase in the number of mixed pixels, where a wide range of depths and surface turbulence occurred within a single pixel. Matched filter (MF) mapping of woody debris generated overall accuracies of 83% in the fifth-order Lamar River. Accuracy figures for the in-stream habitat and wood mapping may have been misleadingly low because the fine-resolution imagery captured fine-scale variations not mapped by field teams, which in turn generated false ''misclassifications'' when the image and field maps were compared.

The use of high spatial resolution hyperspectral (HSRH) imagery for stream mapping is limited by the need for clear water to measure depth, by any tree cover obscuring the stream, and by the limited availability of airborne hyperspectral sensors. Nonetheless, the high accuracies achieved in northern Yellowstone streams indicate that HSRH imagery can be a powerful tool for watershed-wide mapping, monitoring, and modeling of streams.

Keywords: Remote sensing; In-stream habitat; Morphology; Woody debris; Depth; Mountain stream

1. Introduction

Mapping variations in stream habitat, water depth, and woody debris throughout entire watersheds can be

* Corresponding author. Fax: +1-541-346-2067.
E-mail address: marcus@oregon.uoregon.edu (W.A. Marcus).

0169-555X/03/$ - see front matter © 2003 Elsevier Science B.V. All rights reserved.
doi:10.1016/S0169-555X(03)00150-8

notoriously difficult in mountain environments. The paucity or absence of fine spatial resolution, basin-wide maps of stream characteristics poses a major obstacle to understanding how mountain stream processes and responses are integrated into broader, watershed-wide geomorphic systems and are modified by human impacts.

High spatial resolution hyperspectral (HSRH) imagery is a tool potentially capable of acquiring detailed maps over a stream's entire length. High spatial resolution (≤ 5 m) provides the detail necessary to capture key features in the narrow headwater streams typical of mountain environments. The spectral coverage and narrow bandwidths associated with hyperspectral imagery (generally ≥ 64 bands) allow the user to differentiate features of interest that could not be distinguished otherwise. This article evaluates the ability of 1-m, 128-band imagery to map in-stream habitats, stream depths, and woody debris in third- to fifth-order streams of the northern Yellowstone region. If a single remote sensing instrument could be used to map this suite of features at watershed scales, it would simplify data collection, improve access to remote areas, reduce costs, and enable better monitoring and modeling of river habitat in mountain watersheds.

2. Previous research

The early applications of digital remote sensing technology in the context of fluvial systems focused on large rivers or reservoirs, where the water could be clearly delineated using the coarse 10–80-m pixel resolution available from satellites. Since approximately 1990, however, the development and accessibility of airborne sensors (e.g., AVIRIS); improved technology for converting film-based images to digital form; and high spatial resolution satellite-based sensors (e.g., IKONOS) have created new opportunities for applying digital remote sensing to small streams typical of mountain environments. Fourteen sensors with spatial resolutions of ≤ 5 m are scheduled for launch by the year 2005 and imagery from nine of these instruments will be commercially available (Ustin and Costick, 2000).

Research on remote sensing of in-stream features has largely focused on microhabitats, such as pools, glides, and riffles—critical habitats for benthic fauna (Orth and Maughan, 1983). These morphologic units also provide a template for predicting where contaminants might accumulate in stream sediments (Ladd et al., 1998). Hardy et al. (1994) found "close" agreement between ground- and image-based maps of hydraulic features such as pools, eddies, and runs on the Green River, UT, using multispectral video imagery at spatial resolutions of 0.25–3 m. In contrast, in the much smaller third- and fourth-order Soda Butte and Cache Creeks of Montana and Wyoming, Wright et al. (2000) obtained poor results using 4-band, 1-m imagery to map stream habitats, with standard supervised classification procedures producing overall accuracies ranging from 10% to 53%. The inadequacy of their results was largely attributed to coregistration problems, although the need for greater spectral resolution was also noted. To avoid these coregistration issues, Marcus (2002) mapped stream microhabitats in the fifth-order Lamar River of Wyoming directly to hardcopy printouts of 1-m, 128-band hyperspectral imagery to ensure a perfect match between the classified imagery and field maps. Marcus used a maximum likelihood classification approach to achieve an overall classification accuracy of 85%. Using the same imagery and the same field data, Goovaerts (2002) was able to improve the in-stream habitat classification accuracy to 99% using a co-kriging classification scheme.

Both the improved spectral and enhanced spatial resolution provided by HSRH imagery appear necessary to accurately map in-stream habitats. Marcus (2002) found that using 1 m rather than 5-m pixel resolution increased overall accuracies by 19.4% and that using 128 band rather than 4-band, 1-m imagery improved accuracies by 17.6%. Similarly, Legleiter et al. (2002) noted that overall accuracies increased by 7.2% when using 128-band HSRH imagery rather than 8-band imagery and by 4.7% when using 1 m rather than 2.5-m imagery.

Research on remote measurement of stream depth has also received increasing attention from the remote sensing community in recent years. Lyon et al. (1992) classified five depth categories with 95% accuracy using a radiative transfer model with four visible light bands in the relatively large (compared to our study sites) Saint Mary's River of Michigan. The radiative transfer model and resultant depth estimates, however,

were dependent on Secchi Disk measurements of extinction coefficients, an approach that would be difficult or impossible to apply in the comparatively shallow and often turbulent conditions found in mountain rivers. Gilvear et al. (1995) used scanned panchromatic photos with ~ 1-m resolution to differentiate deep versus shallow water, but did not attempt precise depth estimates. A quantitative study by Winterbottom and Gilvear (1997) succeeded in estimating depths with 2-m, 9-band simulated Daedalus AADS imagery, generating R^2 values of 67% for water depths up to 1.2 m. Their cross-section analysis indicated that the 67% figure probably underrepresented the quality of the depth estimates, which produced cross-sections very similar to those surveyed at the same sites.

Active sensors, including radar, have shown greater potential for accurate depth measurements than have passive, reflected signals. In a variety of stream conditions with depths up to 5 m, ground-penetrating radar produced an overall R^2 value of 97% for measured versus estimated depths (Spicer et al., 1997). Ground-penetrating radar also shows great promise as a technique for estimating stream velocities (Spicer et al., 1997; Costa et al., 2000).

In comparison to work on microhabitats and stream depth, remote sensing of wood has received relatively little research attention. Marcus et al. (2002) had relatively poor success using 1-m, 4-band imagery to map wood in Cache Creek in northern Yellowstone Park, largely because of spectral confusion between gravel and wood in mixed pixels and coregistration problems similar to those encountered by Wright et al. (2000). Although readily apparent to the naked eye, the configuration of woody debris (especially when present as isolated logs or small sets of logs) made up such small portions of individual pixels that it often could not be distinguished from the surrounding background, even with 1-m imagery. Marcus et al. (2002) recommended using either finer resolution imagery, which is difficult to acquire, or hyperspectral imagery, which enables objects with a clear spectral signal (like wood) to be distinguished even when they make up only a fraction of a pixel (Boardman, 1989, 1993).

Previous research has demonstrated the potential of digital remote sensing as a tool for mapping key characteristics of small streams. To date, however, the research has focused on using imagery to map one variable, usually within a reach of limited size. Evaluating whether a single instrument can map a suite of critical habitat characteristics indicates how effectively these approaches can simplify and improve watershed-wide mapping of streams. Quantifying variations in mapping accuracy is also required to understand the performance of these techniques at varying stream scales. This article evaluates the potential for using high spatial resolution hyperspectral imagery (HSRH imagery) to map stream microhabitats and depths in third-, fourth-, and fifth-order channels and wood within and on the bars of a fifth-order channel.

3. Field area

We collected hyperspectral imagery and mapped in-stream habitats and depths in August 1999 along two reaches in Soda Butte Creek and one reach in the Lamar River (Fig. 1). Because of time constraints, woody debris was only surveyed in the Lamar Reach. Approximate reach lengths were 2 km for the Footbridge Reach in Soda Butte Creek and the Lamar River and ~ 5 km for the Cooke City Reach. These stream reaches were selected because they are part of long-term studies on stream disturbance and change due to mining (Ladd et al., 1998; Marcus et al., 2001), fire and the associated introduction of woody debris (Minshall et al., 1998; Marcus et al., 2002), and flooding (Meyer, 2001). In addition, portions of these reaches and nearby areas have been used to test the ability of 4-band, 1-m resolution imagery to map in-stream habitats (Wright et al., 2000) and woody debris (Marcus et al., 2002). The following description of these reaches focuses on key factors controlling spectral response and classification accuracy.

All the reaches displayed pool/riffle morphology (Montgomery and Buffington, 1997) with single- to multichannel configurations and well-developed gravel bars. Variations in stream hydraulics were also similar across reaches, with surface turbulence ranging from areas of mixed white water and surface waves in riffles to mirror-like surfaces in glides.

Stream depths in all reaches typically varied between 0 and 0.6 m, with measured maximum stream depths up to 1.6 m in the Lamar River and 1.2 and 1.3 m in the Footbridge and Cooke City

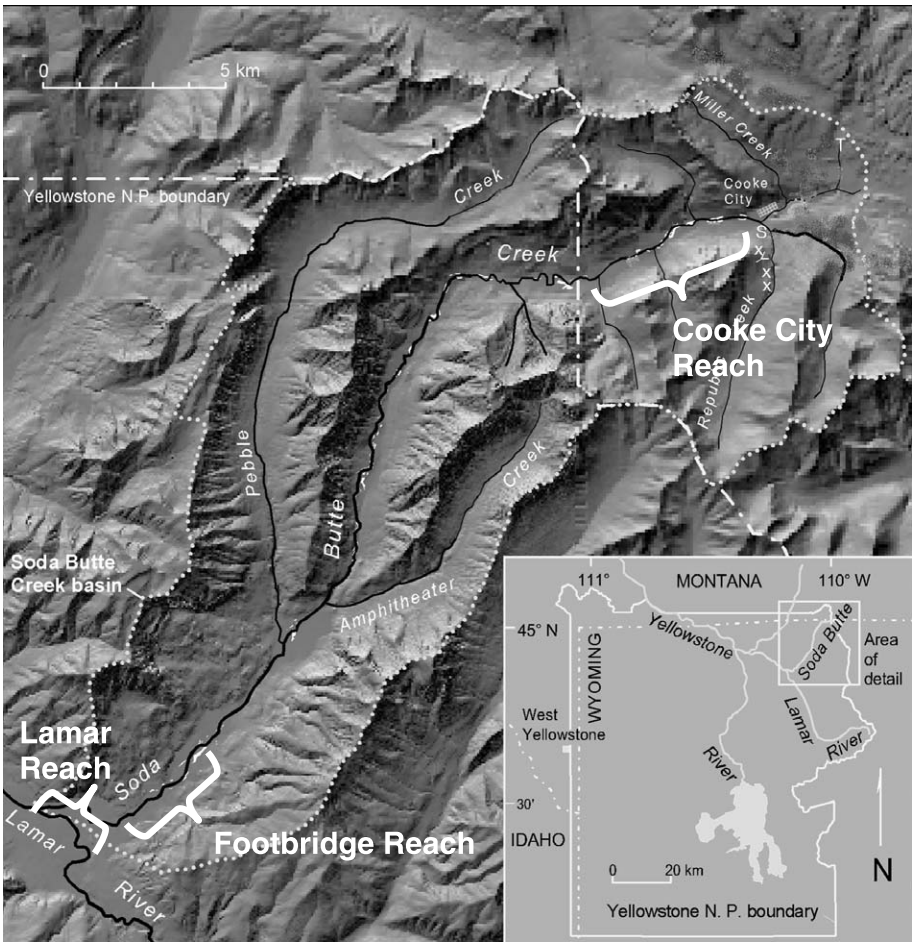

Fig. 1. Location of the three study reaches. Figure modified from Marcus et al. (2001).

Reaches, respectively, of Soda Butte Creek. Water conditions were clear when the spectral imagery was collected, and field crews could easily see the stream bottom at all sites, except in white water riffles.

The substrate in all reaches varied from sand size in eddy drop zones to cobbles in scour pools or high-gradient riffles. Substrate composition in all reaches primarily consisted of sediments from the Eocene volcanics that dominate the northern Yellowstone landscape. Substrate materials from granitic gneisses and sedimentary rocks above Cooke City (Metesh et al., 1999) were also present in Soda Butte Creek, particularly in the Cooke City Reach. The substrate was, for the most part, free of algae when imagery was acquired.

The similarities among stream reaches suggest that major differences in classification accuracies between stream reaches noted in this article most likely result from scale differences and *not* from gross differences in morphology, surface turbulence, substrate, or water column characteristics. The Lamar River reach is fifth-order as determined from USGS 1:24,000-scale topographic quadrangles. Soda Butte Creek is third-order at the Cooke City site and fourth-order at the Footbridge Reach (Fig. 1). Variations in the scale of in-stream features (e.g., the size of riffles or gravel bars) paralleled the variations in stream order, with larger features in higher-order channels. Based on USGS gage records farther downstream, discharge in the Lamar River was ~ 7.1 m^3/s (250 cfs) on 3

August 1999 when imagery was collected. Discharge at a USGS gage on the Footbridge Reach of Soda Butte Creek was 3.9 m^3/s (139 cfs) on 2 August 1999 when imagery was collected. Based on a ratio of discharge to basin area, the discharge at the head of the Cooke City Reach would have been 20% of that at the Footbridge Reach, or ~ 0.79 m^3/s (28 cfs).

4. Methods

4.1. Data collection

Hyperspectral data were collected on 3 August 1999 for the Lamar River and the Cooke City Reach of Soda Butte Creek, and on 2 August 1999 for the Footbridge Reach of Soda Butte Creek. Imagery was collected using a Probe-1 sensor mounted on an A-Star Aerospatiale helicopter flying 600 m above the ground surface. The Probe-1 measured reflected energy across 128 contiguous bands covering the visible to shortwave–infrared portions of the spectrum (0.438–2.507 μm) with a spectral bandwidth of 0.016–0.020 μm.

The digital data were downloaded the day of the flight and printed out as true color composites. Field teams mapped depths and in-stream habitats directly to the imagery within 10 days of the overflight. The field teams mapped seven types of habitat units based on the Bisson et al. (1982) scheme that is widely used by fisheries biologists and management agencies. In addition, in the Footbridge and Cooke City Reaches, we mapped a category we called standing water, which referred to shallow pools cut off from the main channel. We later merged the high- and low-gradient riffles into one category called riffles, merged glides, runs, and rough-water runs into one unit called glides, and merged standing water and eddy drop zones into one unit called eddy drop zones, leaving us with four in-stream habitats: pools, glides, riffles, and eddy drop zones (Fig. 2). The use of this simplified four-unit classification system significantly reduced field mapping errors that resulted when different surveyors mapped the same type of unit (e.g., a run) in different

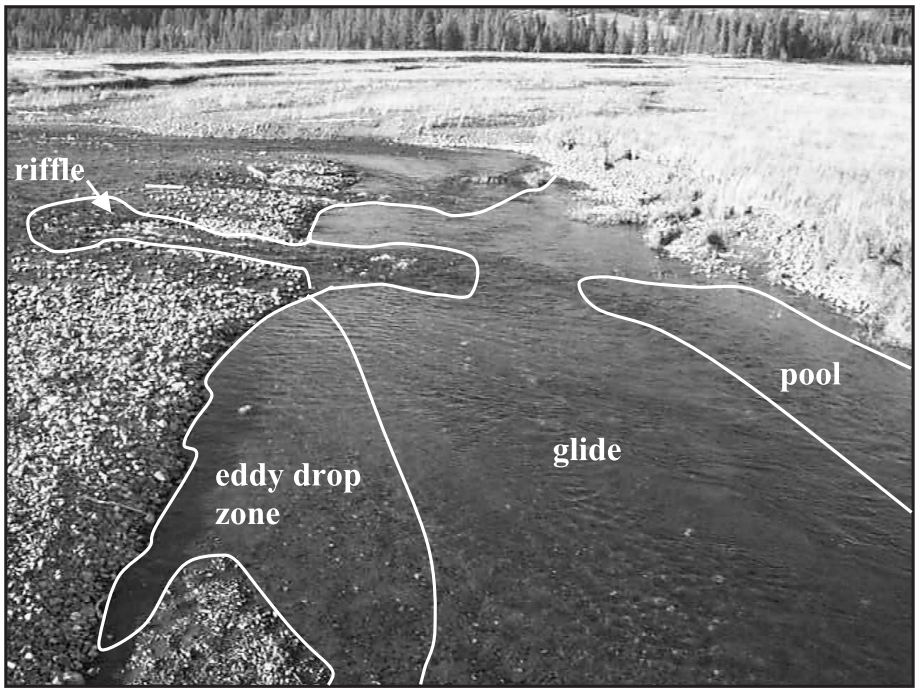

Fig. 2. The four types of in-stream habitats mapped in Soda Butte Creek and the Lamar River. The boundaries between units are often transitional and usually require subjective mapping decisions by the field teams. Photo from Soda Butte Creek immediately downstream of Pebble Creek, November 1999.

ways (e.g., as a run or as a glide or as a rough-water run) (Marcus, 2002). Removing these disagreements in field mapping was critical because such inconsistency would have confused subsequent accuracy assessments of image-based maps and made it difficult to determine whether classification errors indicated limitations of the imagery or subjectivity in the ground ''truth'' maps produced by field teams. More detailed descriptions of these unit types are provided in Ladd et al. (1998), Wright et al. (2000), Marcus et al. (2002), and Legleiter et al. (2002).

Depths were mapped at points that could be clearly located on both the image printouts and in the field. We attempted to measure at least one depth in each individual habitat unit (e.g., one point in every pool in a given reach). Depths were measured using a ski pole calibrated in 5-cm increments.

Woody debris in the Lamar River was mapped on 10–12 November 1999. Time and logistical constraints prevented field mapping of wood in other reaches. No flows that were capable of moving the wood occurred between the time of image acquisition and field mapping. Wood was mapped directly to true color printouts of the images to ensure precise coregistration of imagery and maps. We only mapped those pieces of wood longer than 2 m, >10 cm in diameter, and clearly visible on the imagery.

4.2. Data analysis

All remote sensing analysis was conducted in Environment for Visualizing Images (ENVI), a remote sensing software package. Field maps were digitized on-screen from the hard copies used in the field. Because imagery for the various reaches was collected at different times of day with different lighting conditions, we based analyses for each reach on training data from the same reach. Using training sites from Cooke City, for example, to generate classifications in the Lamar River was not appropriate given the variations in sun angle between images. Classifications were entirely spectrally driven; other types of data (e.g., texture measurements) were not used. Analyses specific to in-stream habitats, depths, and wood are presented in the following sections.

4.2.1. Image preprocessing

Because depths and in-stream habitats were mapped directly to printouts of the raw imagery within several weeks of the flight, we did not attempt to georeference the imagery to correct for image distortion. Subsequent coregistration of field data and imagery used the pixel x, y coordinates of the imagery. The absence of geographic coordinates did not affect the field mapping or classification techniques we used, but would be an obstacle to integrating the classification maps into GIS analyses with other data layers. Following straight flight lines paralleling the stream's course and continuously running the Probe-1 sensor's cross track scanner provided images 2–6 km in length. Each study reach, therefore, fell entirely within a single image and, unlike applications using along track scanners, we did not need to mosaic a

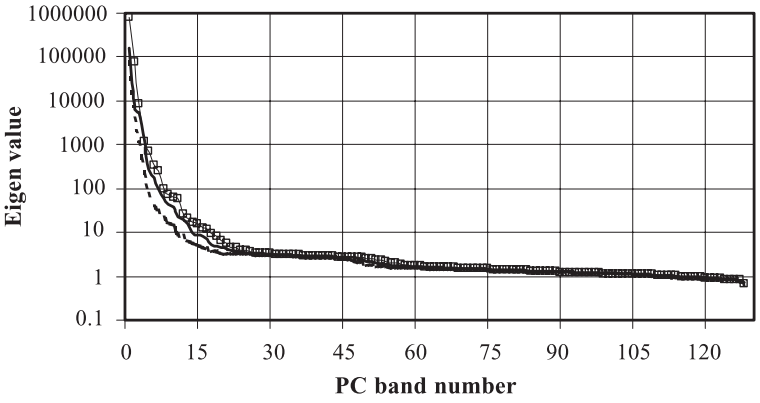

Fig. 3. Eigenvalue plots of the eigenvalues for the 128 principal components for the Lamar River (dashed line) and the Cooke City Reach (solid line with squares) and Footbridge Reach (solid line) of Soda Butte Creek.

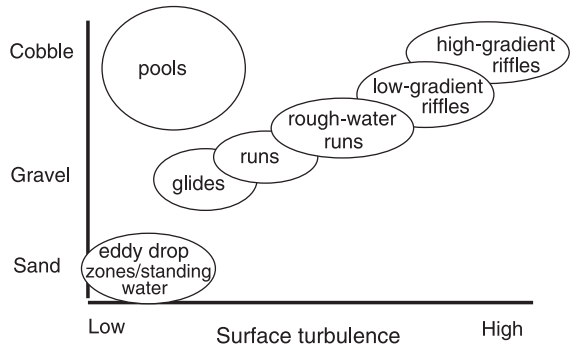

Fig. 4. A schematic diagram of the general relation of morphologic units to substrate size and surface turbulence of the water.

number of separate scenes. The data were not atmospherically corrected.

4.2.2. In-stream habitats

Field crews mapped in-stream habitats as polygons that covered the entire stream. This article reports on the results for classifying all the stream pixels that were mapped as well as a spatially buffered version of the original field map polygons. Spatial buffers were applied because most boundaries between units were fuzzy, with one unit (e.g., a riffle) gradually transitioning into the next (e.g., a glide) over a distance of several meters. Removing a buffer zone where these transitions occurred better represented the reality of the stream environment.

Generating image-based classifications required several steps. All nonstream areas were first masked out. We then transformed the image data using a nonstandardized, principal component algorithm to minimize spectral noise and to reduce the number of bands required for classification, a standard technique in hyperspectral analysis. We used variance-based PCA images rather than correlation-based PCA because the variance-based images generated higher classification accuracies. Classifications for each reach were conducted using a maximum likelihood supervised classification based on training sites from the same reach. This maximum likelihood principal component approach generated the best results among the numerous techniques we investigated and is, therefore, the focus of this article.

The classification was developed using 129 randomly chosen training sites from each feature type in each reach. The minimum number of training sites required for a maximum likelihood supervised classification was 129 with 128 spectral bands as input (Richards, 1994).

Eigenvalue plots (Fig. 3) indicated that over 100 of the 128 principal components contributed significant information (i.e., eigenvalue >1.0), but the highest overall classification accuracies and kappa coefficients were generated using only the first 25 PC bands in the Lamar River, the first 20 in the Cooke City Reach, and the first 15 in the Footbridge Reach. Classification accuracies gradually decreased as additional PC bands beyond this optimal number were used for the classification (Marcus, 2002), presumably because these additional bands included increasing amounts of residual noise from the original images.

Table 1
Error matrix for maximum likelihood supervised classifications of in-stream habitats using principal component images derived from 128-band hyperspectral imagery[a]

Image classification	Ground truth (number of pixels)				
	Glides	Riffles	Pools	Eddy drop zones	Total
Third-order, Cooke City Reach					
Glides	**2574**	424	51	7	3056
Riffles	496	**550**	115	21	1182
Pools	191	30	**95**	2	318
Eddy drop zones	161	56	19	**62**	298
Total	3422	1060	280	92	4854
Fourth-order, Footbridge Reach					
Glides	**6152**	561	25	10	6748
Riffles	2020	**1047**	11	0	3078
Pools	151	16	**94**	0	261
Eddy drop zones	7	0	0	**22**	29
Total	8330	1624	130	32	10,116
Fifth-order Lamar River Reach					
Glides	**6083**	389	12	77	6561
Riffles	174	**2653**	6	23	2856
Pools	323	313	**132**	1	769
Eddy drop zones	139	142	2	**564**	847
Total	6719	3497	152	665	11,033

[a] A two-pixel (~2 m) spatial buffer has been removed from the perimeter of each unit prior to accuracy assessment. Columns show the number of pixels in a given class as mapped by the field team, and the rows show the number of pixels in a given unit as classified by the image. For example, 3422 total pixels were field mapped as glides, of which 2572 were classified as glides on the image, 496 as riffles, 191 as pools, and 161 as eddy drop zones. Data for the Lamar River from Marcus (2002). Bolded values indicate number of pixels correctly classified in each category.

Table 2
Summary of classification accuracies for Soda Butte Creek and the Lamar River[a]

Reach	Buffer size (m)	Number of PC bands	Overall accuracy (%)	Kappa coefficient	Producer's and user's accuracies (%) for:							
					Glides		Riffles		Eddy drop zones		Pools	
					Producer	User	Producer	User	Producer	User	Producer	User
Cooke City	2	20	67.6	0.35	75.2	84.2	51.9	46.5	33.9	29.9	67.4	20.8
Cooke City	No buffer	NA	NA	NA	NA	NA	NA	NA	NA	NA	NA	NA
Footbridge	2	15	72.3	0.31	73.8	91.2	64.5	34.0	68.8	75.9	72.3	36.0
Footbridge	No buffer	15	62.0	0.29	67.1	67.1	49.7	49.7	77.9	15.8	33.6	30.2
Lamar	2	25	85.5	0.74	90.5	92.7	75.9	92.9	84.8	66.6	86.8	17.2
Lamar	No buffer	25	65.6	0.40	67.6	90.1	59.5	67.2	84.7	7.8	68.9	10.2

[a] Data for the Lamar River classification from Marcus (2002) using a 2-m buffer zone. Producer's accuracy refers to the accuracy that the producer of the original field maps can calculate by overlaying the pixels classified as a particular feature (e.g., glides) on the ground map of that feature. The producer's accuracy is the percent of the ground truth map that is correctly classified for all ground-mapped pixels of a given feature. The user of the classified image does not have the original ground truth map and therefore must check the accuracy by going to all sites in the field classified as a specific feature type (e.g., a glide). The user's accuracy is the percent of the image map that is correctly classified for a given feature. See Congalton and Green (1999) for a more detailed explanation.

Table 3
Step-wise multiple regression results for depth (y) versus values of different principal component scores (x_1, x_2,. . .,x_n) for each pixel where depth was measured[a]

Location of depth measurements	Number of sites	Order of principal component bands included in regression	Adjusted R^2 (%)	Predicted R^2 (%)
Lamar Reach, 5th order				
All sites combined	175	7, 3, 22, 15, 25, 28, 11, 21, 23, 4, 26	44.0	38.3
Eddy drop zones	9	23, 29, 4	93.2	88.9
Pools	23	23, 225, 15, 28, 12, 10, 13	85.1	78.4
Glides	60	7, 19, 3, 11, 27, 25, 17, 21	41.6	28.7
Runs	33	20, 15, 14, 13, 26, 25, 224, 24, 22, 27, 28, 17	88.3	79.4
Low-gradient riffles	29	3, 22, 12, 4, 17, 20, 9, 1	79.8	66.3
High-gradient riffles	16	11	20.0	0.00
Footbridge Reach, 4th order				
All sites combined	144	4, 2, 11, 5, 7, 6	27.9	23.9
Standing water	11	10, 20, 19, 22, 14, 15	99.6	99.1
Eddy drop zones	13	4, 11, 20, 17, 10, 9	91.0	79.2
Pools	7	21	45.3	21.9
Glides	22	5, 13	42.6	31.5
Runs	50	26, 30, 22, 20, 7, 6, 8, 0, 21	43.6	26.6
Low gradient riffles	21	7, 3, 24, 28, 11, 19, 2, 30	79.3	54.5
High gradient riffles	15	11, 16	72.2	66.0
Cooke City Reach, 3rd order				
All sites combined	105	2, 4, 1, 10, 9, 3, 11, 8, 5	59.0	53.4
Eddy drop zones	17	2, 4, 9, 11, 14, 1, 13, 8, 10	93.8	80.9
Pools	5	1	72.3	0.0
Glides	17	1, 7, 3, 5, 13, 15, 6, 10, 2, 9, 8	98.6	90.0
Runs	9	2, 1, 5, 3	93.1	76.7
Rough water runs	10	3, 2, 9	82.5	55.1
Low gradient riffles	11	2, 8, 5, 1, 3	91.7	83.0
High gradient riffles	35	2, 1, 4, 17, 9, 18	67.0	55.4

[a] Only PC scores significant at $p \leq 0.10$ are entered into the regression. High R^2 values are suspect because of small sample sizes (i.e., small number of sites), but results indicate that stratifying by morphologic units has potential as a means for improving depth predictions with HSRH data.

Classification accuracies reported in this article represent the maximum accuracies achieved when the optimal number of PC bands were used.

Accuracy assessment followed standard confusion matrix procedures, as outlined by Congalton and Green (1999). Pixels used in the training set were not used for evaluating classification accuracy.

4.2.3. Depth analysis

Depth analysis was conducted on the same principal component images used for the in-stream habitat analysis. All depth sites within each reach were entered into a stepwise multiple regression to determine the strength of the relationship between depth and spectral reflectance and to develop equations for estimating depths throughout the stream. Because variations in spectral reflectance within a reach at a given time are a function of surface turbulence and substrate composition as well as depth, we used the spectral classification of in-stream habitats to stratify the sample by morphologic unit. High-gradient riffles, for example, tend to have similar surface turbulence and substrate characteristics at all locations within a reach, thus reducing the variation in those factors and isolating depth as the primary driver of the observed spectral reflectance.

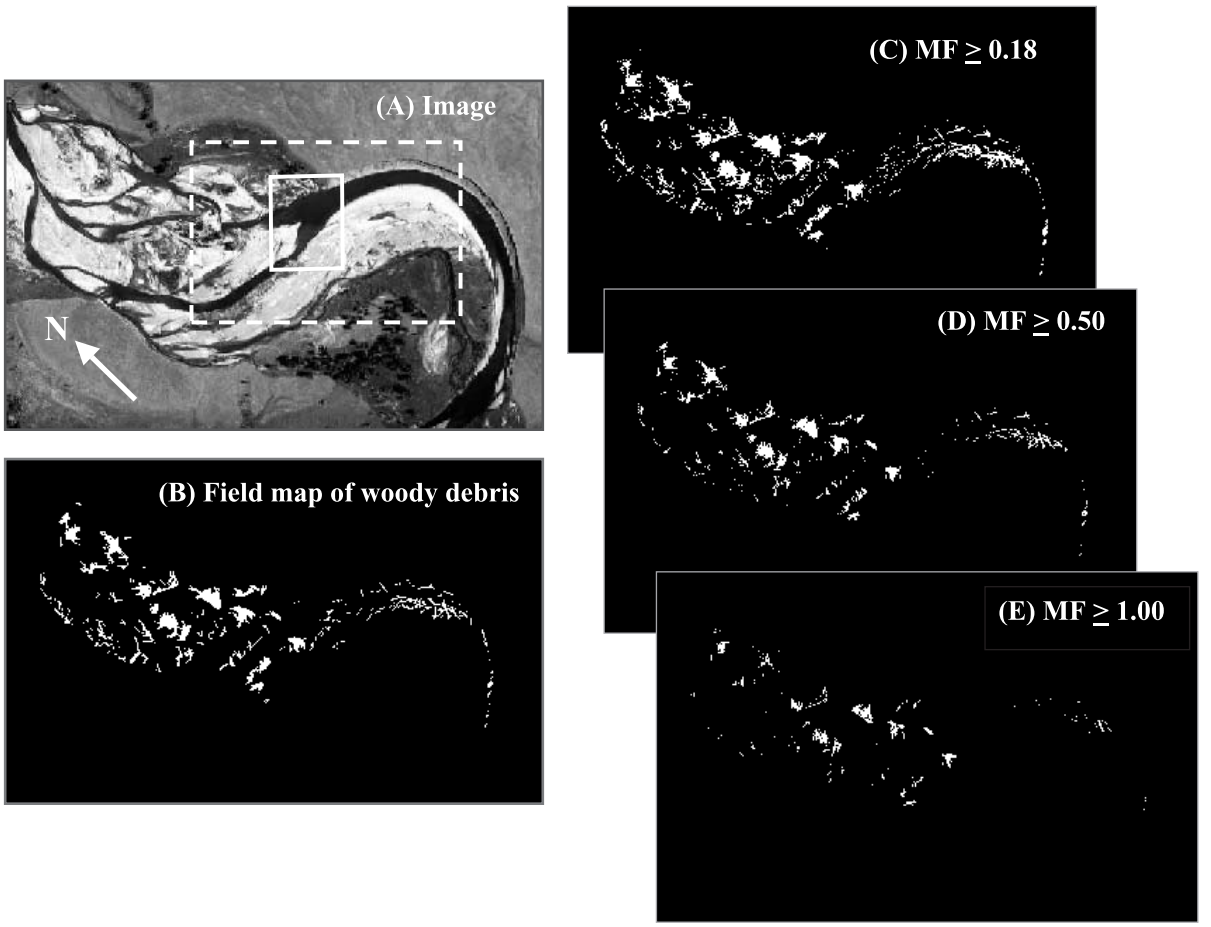

Fig. 5. Woody debris mapping in the upper 0.75 km of the Lamar River Reach. (A) Field teams mapped wood directly to a printout of the original image. Training pixels (129) were randomly selected from the (B) field map and a matched filter process was applied to generate threshold images. Shown in white are pixels that equal or exceed a threshold value of (C) 0.18, (D) 0.50, or (E) 1.00 on the matched filter image. Choice of the appropriate threshold value is partly a subjective decision, as is discussed in the text. The solid white box in (A) corresponds to the location of the image shown in Fig. 6; the dashed box shows the location of the depth map in Fig. 7.

For purposes of depth analysis, we used the original eight in-stream habitats (high- and low-gradient riffles, eddy drop zones, standing water, rough-water runs, runs, glides, and pool) rather than merging the units into riffles, glides, pools, and eddy drop zones as was done for the mapping of in-stream units. Use of the eight units better stratified the stream by surface turbulence and substrate size, although some overlap between units was present (Fig. 4). Stratifying the sample using the image-based classification of in-stream units rather than our field maps provided a better indication of the potential of the technique to be applied in areas where field teams are not available to generate detailed ground maps prior to using the imagery for depth analysis.

4.2.4. Wood analysis

Procedures for classifying wood initially followed the same techniques used for in-stream habitats. A mask was used to remove features outside the exposed bars where wood was located. We then performed a principal component transformation on the remaining portion of the image.

We used the matched filter (MF) approach in ENVI to identify woody debris in the principal component image. The MF algorithm performs a partial unmixing of spectra to estimate the relative quantity of a given material in a pixel based on user-defined spectral end members (wood in this case) (Harsanyi and Chang, 1994; Boardman et al., 1995). Matched filtering has the advantage of not requiring knowledge of all end members within an image scene and so can be used to identify single feature types. The MF technique created an image that assigned values to each pixel, with high values indicating more wood-like features.

Normally, one selects a pure pixel or set of pure pixels to train a matched filter image, but this generated poor classification results for wood. We therefore selected 129 pixels that were equally distributed around the image in wood of all sizes, ranging from individual logs to large debris jams.

5. Results

Table 1 shows error matrices for in-stream habitat mapping using a 2-m spatial buffer and principal component images. Table 2 depicts the variations in overall accuracies, kappa coefficient values, and producer's and user's accuracies among the three reaches and between buffered and unbuffered units. Overall classification accuracies are 67.6% for the third-order reach, 72.3% for the fourth-order reach, and 85.5% for the fifth-order reach. Use of the spatial buffer to remove transitional areas along unit boundaries increases accuracies by 10.3% in the fourth-order Footbridge Reach and 19.9% in the fifth-order Lamar Reach.

The results of the stepwise multiple regression relating depths to non-normalized principal component scores for the hyperspectral data are shown in Table 3. R^2 values when all the depth data are pooled together for each reach range from 27.9% in the Footbridge Reach to 59.0% in the Lamar River. When the depth data are stratified by in-stream habitat type,

Table 4
Changes in wood mapping accuracy in the Lamar River Reach as different matched filter minimum threshold values are applied[a]

Minimum threshold value	Overall accuracy (%)	Accuracy measures for wood only				
		Error of commission (%)	Error of omission (%)	Producer's accuracy (%)	User's accuracy (%)	# of pixels classified as wood
mf>0.18	93.4	39.7	15.3	84.7	68.1	12,638
mf>0.20	94.1	33.5	16.3	83.7	71.4	11,897
mf>0.23	94.7	26.5	18.2	81.8	75.5	11,002
mf>0.25	95.0	22.7	19.5	80.5	78.0	10,477
mf>0.35	95.4	12.0	26.9	73.1	85.9	8638
mf>0.50	94.9	3.9	38.7	61.3	94.0	6620
mf>0.75	93.0	0.6	57.8	42.2	98.5	4354
mf>1.00	91.2	0.2	73.4	26.6	99.3	2722

[a] Only two classes were mapped for purposes of this analysis: wood and nonwood. The field team mapped 10,153 wood pixels on the ground truth image (Fig. 4).

adjusted R^2 values vary widely, ranging from 20.0% for high-gradient riffles in the Cooke City Reach to 99.6% for standing water in the Footbridge Reach.

Fig. 5 portrays a black-and-white composite image of the area where wood was mapped, the field map of wood, and wood classifications based on matched filter analysis using different minimum thresholds. Table 4 shows the changes in different accuracy measures that occur as different threshold values are used. The implications of using different thresholds are discussed below.

6. Discussion

The following sections on in-stream habitats, depth, and woody debris discuss issues specific to each parameter. We also describe factors affecting mapping accuracy, possibilities for improving classification results, extensions of HSRH mapping to watershed scales, and future research directions. The section concludes with some general comments that apply to HSRH mapping of these three important stream parameters.

6.1. In-stream habitats

The ability of HSRH imagery to classify in-stream habitats varied with stream scale. Overall and producer's accuracies consistently improved as stream order increased (Table 2). The greater accuracy in the fifth-order Lamar River probably occurred because larger streams feature more sizable, more homogenous units than do smaller streams. This, in turn, significantly reduced the proportion of the stream occupied by transitional boundary areas between in-stream habitats as well as the amount of internal variability displayed within a single unit (e.g., small riffle-like areas within a glide).

The application of the 2-m buffer improved classification accuracies (Table 2) by removing a portion of the transitional boundary zone that is difficult to map in the field. Even with the 2-m buffer, however, image-based classifications often displayed a mix of unit types on the margins of individual units. These regions generated apparent classification errors when compared to the homogenous ground-truth polygons mapped by field teams.

One approach to resolving the discrepancies between homogenous ground truth maps and heterogeneous classifications would be to use post-classification filters that "clump and sieve" the classified pixels to create more cohesive classification units. This post-classification fix would ignore, however, the possibility that the concentration of pixel-scale heterogeneity at unit boundaries on the image maps is real; i.e., that the imagery may provide more accurate and precise maps than the ground teams (Marcus, 2002; Legleiter et al., 2002). For example, close examination of Fig. 6 shows a scattering of riffle and glide pixels near unit boundaries, suggesting that the imagery detected subtle variations where surface roughness is locally riffle-like, but glide-like only a few centimeters away. Such variations are indeed observed in the field, but ground teams could not map at this scale because of time limitations and the difficulty of precisely locating the pixel on the image. The field team's placement of unit boundaries through these transitional areas was also somewhat arbitrary.

The image classification also indicates shoreline boundary effects that make sense from a hydraulic perspective. Areas mapped as riffles by the field team are shown by the imagery to have glide pixels near the shoreline; a feature that occurs as water shallows and slows at stream edges (Fig. 6). Eddy drop zones are shown immediately adjacent to the shore, where water velocity drops to nearly zero and sands and silts are deposited along the banks. These features, however, were too small to be mapped in the field.

Two primary sources of ground survey error therefore probably led to discrepancies between field maps and image-based maps: (i) inconsistent identification of units by field crews; and (ii) lumping of small regions of variability (e.g., a small riffle) into a larger more homogenous region (e.g., a glide). Based on this rationale and on our experience with the field sites, we believe that the HSRH maps were more consistent and precise in their characterization of unit boundaries and heterogeneity than the large, homogenous polygons created by the field teams. If this is the case, then the poorer classification results in the Cooke City Reach may not reflect a weakness of the classification capabilities of HSRH imagery in lower-order streams, but a weakness of the techniques used to field map and validate the image classifications in these tremendously variable environments.

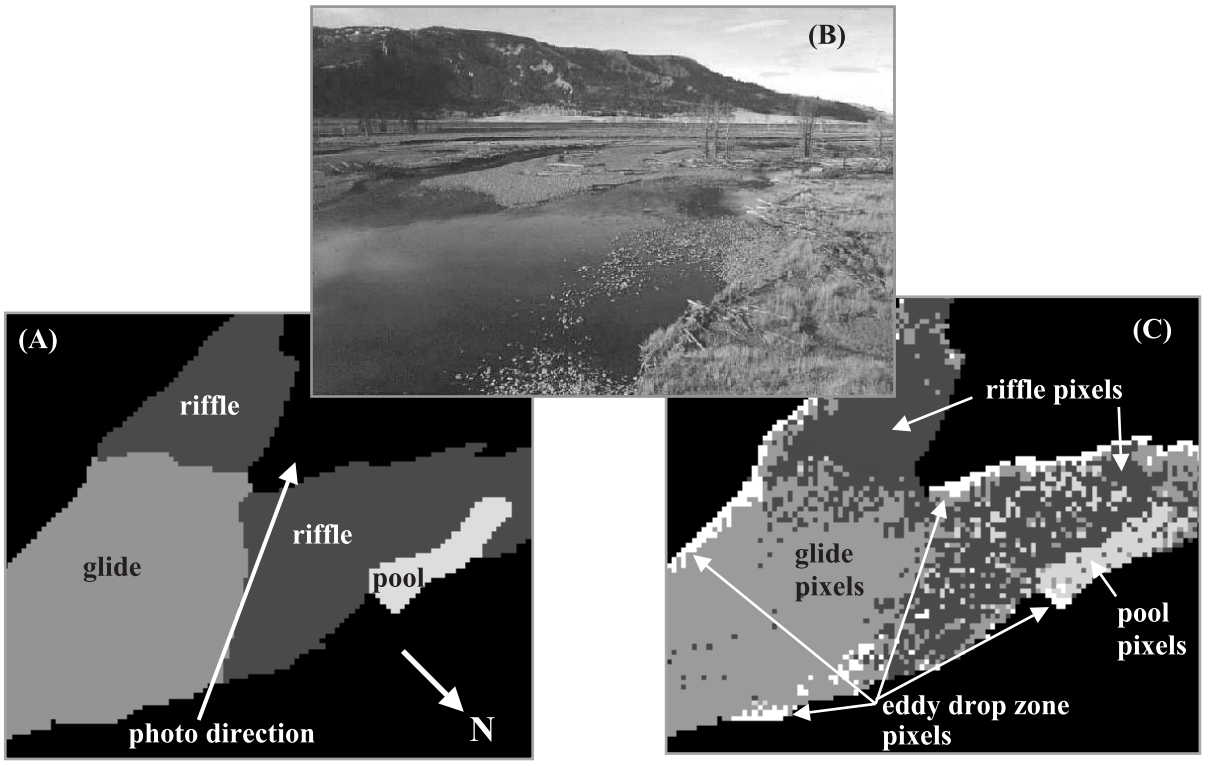

Fig. 6. (A) The field map of in-stream habitats, (B) a photo looking downstream at the same location 3 months later when water levels had dropped and the extent of the riffles had decreased, and (C) the HSRH classification of the same location. Eddy drop zones were not mapped by the field team in this area because they were below the minimum mapping size, but the HSRH imagery designated shallow shoreline areas that were often covered with silt and sand as eddy drop zones. The riffle on the right channel is portrayed as having a mix of riffle, glide, and deeper water pool units, which is also a realistic portrayal of that particular location. The location of these images is shown by the solid white rectangle in Fig. 5A.

Future work could evaluate the role of surveyor subjectivity by comparing maps generated by different individuals at the same location, or by revisiting sites using a GPS to pinpoint locations, assuming that precision geocoding can generate meter-scale accuracy in image coordinates. Evaluating the role of spatial heterogeneity in driving classification error would be more difficult, requiring mapping of stream habitats at submeter precision and coregistration of these ground maps to imagery with submeter precision. This level of precision might be obtained using registration panels laid out in the field prior to the image collection flight. We attempted to establish ground control points of this type using 2×2 m blue plastic tarps. Unfortunately, the portions of the images showing the tarps were unusable because of shadowing, image swirl, and line skip. Furthermore, the number of tarps needed to establish adequate ground control can be daunting, especially in a popular, yet relatively pristine locale such as Yellowstone National Park, where special care must be taken to avoid disrupting either the perceived or real natural environment. In sites like Yellowstone, registration panels cannot be left in the field for long periods. There are significant logistical costs, personnel requirements, and disruptions of team morale caused by emplacing and removing registration panels on a constant basis as the team awaits flights that are rescheduled or canceled for various reasons (Aspinall et al., 2002).

Although we believe that the HSRH classifications provide relatively accurate maps of the in-stream habitats at all stream scales, the validation results (Tables 1 and 2) call into question whether this technique is ready for watershed-wide applications,

especially in smaller streams. In particular, although the producer's accuracies for the 2-m buffered units typically approached or exceeded the 85% criteria often considered acceptable for remote sensing classifications, the user's accuracies were often notably lower, especially for the smaller units (pools and eddy drop zones) that make up a small portion of the total stream area (Table 2). Unfortunately, these small pool and eddy drop zone units are often most important as fish habitat and sites of contaminated sediment accumulation (Ladd et al., 1998), making these the features managers are most interested in mapping.

A number of options are available for improving the classification accuracies at all scales. Scaling the size of the spatial buffer to the stream size, for example, could remove more of the confusion caused by transitional zones between units. For example, one might apply a 4-m buffer in the Lamar, a 3-m buffer in the Footbridge Reach, and a 2-m buffer in the Cooke City Reach. This has the disadvantage, however, of not classifying increasingly larger areas of the river as stream size grows. Developing clearer criteria for field mapping boundaries of habitat units might also improve accuracies by ensuring consistency amongst field maps and subsequent selection of training sites for image classification. Fuzzy classifications (e.g., Wright et al., 2000) may be particularly appropriate for mapping the transitional boundaries and characteristics of in-stream habitats. Finally, more sophisticated classification algorithms that take advantage of the tremendous spatial information available in HSRH imagery will improve classification results for in-stream units (Goovaerts, 2002; Maruca and Jacquez, 2002).

6.2. Stream depths

The adjusted R^2 values for depth predictions stratified by in-stream habitat (Table 3) are generally higher than those previously obtained with passive sensors, although lower than those achieved with radar (Spicer et al., 1997; Costa et al., 2000). Except for the glides and high-gradient riffles in the Cooke City Reach, the R^2 values in all three reaches were higher for individual units than when all sites were combined, suggesting that stratification may be useful in other settings as well.

The high R^2 values suggest that HSRH imagery has promise as a tool for estimating depths in clear water streams with no overstory. But the small sample sizes (Table 3) call into question the validity of the analysis from a statistical perspective. This concern can be partially addressed by examining a depth map generated from the regression equations (Fig. 7). This

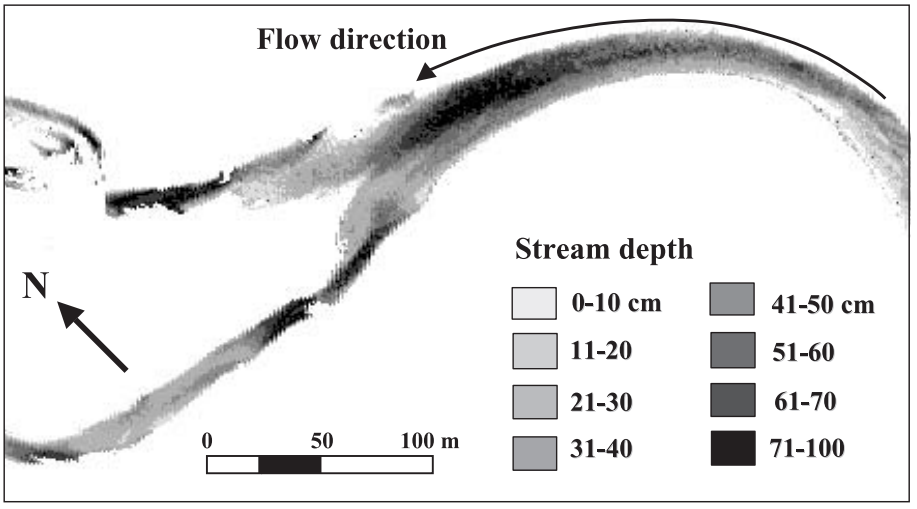

Fig. 7. A depth map of the upper end of the Lamar River Reach, WY. Depths are derived from the stepwise multiple regression equations that relate depth to principal component values for the hyperspectral imagery. Apparent gaps in the stream channel are areas where woody debris overlies the channel and blocks the sensor view of the water. The location of this reach in the upper Lamar River is shown by the dashed white line in Fig. 5A.

map is hydraulically reasonable, with depths that are consistently deepest in the thalweg, cut banks of meander bends, or areas of flow convergence and channel scour. Likewise, the map shows shallow depths along the inside of bends and in areas of flow divergence. Depth ranges displayed by the map are in close agreement with those that occurred in the stream.

The accuracy of depth estimates did not vary in a consistent manner between the stream reaches, although the poorest R^2 values all occurred in the lower-order streams. The lower values in smaller streams may have been driven by the relative increase in the number of mixed pixels, where a wide range of depths and surface turbulence occurred within a single pixel. Stream size will put a bounding limit on the ability of this depth detection technique to work because it cannot be applied in streams that are small enough for banks or overstory to block the sensor's view of the water.

The greatest influence on the accuracy of the technique appears to be surface turbulence, with greater surface turbulence interfering with the sensor's ability to penetrate the water and provide accurate depth estimates. For the most part, units with little surface turbulence (pools, eddy drop zones, and standing water) displayed higher R^2 values. R^2 values for other units did not vary in a consistent fashion, although high-gradient riffles (the most turbulent of the units) had the lowest R^2 values in the Cooke City and Lamar Reaches.

The principal component scores most strongly correlated with depth (i.e., the first scores entered into the stepwise regression) did not follow the rank order of the principal components. Apparently, the signal related to depth is captured within subtle variations in the spectral reflectance of the water. Combined with the large number of principal component scores required to achieve high R^2 values, this emphasizes the desirability of hyperspectral rather than multispectral imagery. In addition, HSRH imagery is necessary to accurately classify the in-stream habitats (Marcus, 2002; Legleiter et al., 2002), a key step in stratifying the stream data in order to improve accuracy.

Finally, the creation of continuous depth maps like Fig. 7 raises the exciting possibility of creating continuous maps for shear stress and stream power. This could be accomplished by coregistering depth maps with high-resolution DEM-based maps of bed slope or, alternatively, by measuring water surface slopes from radar or lidar imagery. Such maps developed at watershed scales would be remarkably valuable tools for understanding stream habitats and disturbance impacts, predicting channel change, and providing the empirical data needed to create and evaluate thermodynamic theories about the distribution of energy expenditure in fluvial systems.

6.3. Woody debris

The data in Fig. 5 and Table 4 indicate that wood can be readily identified on hyperspectral imagery. When evaluating a two-class system (wood and nonwood in this case), no single-matched filter threshold value provided the "best" accuracy. Data from Table 4 suggest, for example, that 1.0 would be the best threshold value for minimizing errors of commission, which occur when nonwood areas are classified as wood. A value of 1.0, however, maximizes the errors of omission, which occur when wood pixels are classified as nonwood. Similar arguments can be made for producer's and user's accuracy, where choosing a high threshold value of 1.0 ensures that almost every image map pixel visited by a user will be wood, but also misses many of the wood pixels mapped by field teams (i.e., the producers of the data). The choice of a threshold will ultimately depend on the map maker's and map user's willingness to accept certain types of error.

We believe that wood, because of its strong spectral signature, can be detected even when it covers only a portion of a pixel. For example, a pixel with a matched filter threshold value of 0.75 and above might represent a pixel covered entirely by wood, while a value >0.18 but <0.25 might represent a pixel with 20% wood coverage. This raises the strong possibility that many pixels identified as errors of commission in the accuracy analysis (Table 4) were in fact pixels that contained wood, but wood that was smaller than the minimum mapping unit used by field teams (Fig. 8). As is the case with the in-stream habitats, this suggests that the image map may be more accurate than the field map that was used to ground truth the imagery.

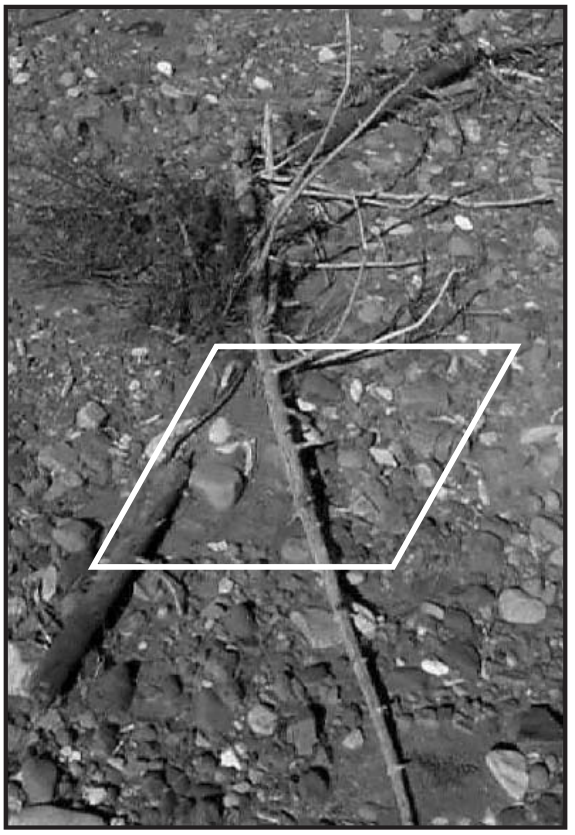

Fig. 8. Wood in the Lamar River Reach that was smaller than the minimum size (2 m long and 10-cm diameter) mapped by field teams. Even though wood of this size was not mapped by field teams, it was probably sensed by the hyperspectral imagery and shows up on matched filter maps (Fig. 5), creating false errors of commission in the accuracy analysis. The footprint of a hypothetical 1-m pixel is shown in white.

The results depicted in Fig. 5 and Table 4 indicate that hyperspectral imagery has great potential as a tool for mapping woody debris, especially at watershed scales where the personnel, cost, and time required for ground mapping can be prohibitive. The only significant logistical obstacles to image-based mapping of wood occur when wood is obstructed by water, vegetation, or shadows.

Several issues should be addressed, however, to improve validation procedures and classification accuracies. The greatest difficulties we encountered resulted from line skip, line oversampling, and image swirl created by platform motion, all of which combined to make it impossible to accurately georeference the image (Aspinall et al., 2002). This concern was partially bypassed by only mapping wood that could be clearly identified on printouts of the imagery. This approach, however, did not permit field mapping of wood smaller than what could be seen on the imagery, which in turn limited the effectiveness of accuracy assessment techniques. In particular, we could not match areas where subpixel wood coverage was indicated by the matched filter image (e.g., Fig. 5C) to corresponding ground sites (e.g., Fig. 8), because the image and ground coordinates could not be coregistered to pixel-scale resolution. Future wood mapping should be done using high quality geocorrected imagery. Corrections at this precision can be accomplished using ray tracing methods for post-correction (Boardman, 1999).

The wood classification worked best when using pixels scattered throughout the image as training sites, rather than when using one or a small number of pure pixels, which is the more standard approach with matched filters. We speculate that the scattered pixel approach worked better because (i) woody debris is heterogeneous, with some that has bark, some that is burned, some that has foliage, and so on; and (ii) the 1-m imagery was not corrected for bidirectional reflectance, so that a series of points from across the entire image captured the range of image spectra for wood better than spectra from just one or two sites. This suggests that segregating the wood by attribute (with or without bark, burned or not burned, with or without foliage, etc.) should improve wood detection by providing purer spectral signatures on which to train the matched filter. In addition, atmospheric correction and removal of bidirectional reflectance both might improve the detectability of wood.

6.4. General considerations

Regardless of the parameter being mapped, we encountered a number of difficulties with image acquisition and processing that are likely to plague any research team using HSRH imagery (Aspinall et al., 2002). Coordination of overflights with field teams was remarkably difficult given the dependence on weather, stream conditions, availability of hyperspectral sensors, and the large number of people that must be mobilized to collect sufficient ground data in a timely fashion. Accurate, pixel-scale georeferencing

and coregistration of imagery and ground data were not possible with submeter-scale precision. Finally, bidirectional reflectance created particular problems with high spatial resolution imagery because the narrow swath width of the cross track scanner (~ 500 m at 1-m pixel resolution with the PROBE-1 sensor) made it difficult to keep the streams near the center of the flight line.

The difficulty in realistically evaluating the accuracy of pixel-scale variations shown on the imagery for in-stream habitats and for subpixel variations in wood indicates that alternative means for accuracy assessment are needed. Accuracy assessment for both wood and in-stream habitat mapping could benefit from (i) pixel-scale ground mapping coupled with use of techniques that provide pixel-scale accuracy in coregistering images and field maps (e.g., Clark et al., 1998; Boardman, 1999); and (ii) the development of techniques that enable realistic comparisons between the pixel- and subpixel-scale variations shown on images and the field maps with their large, homogenous polygons or one class per pixel portrayal of the surface (Aspinall, 2002). Mapping of in-stream habitats in particular will benefit from spatial models that aggregate pixel-scale variations into larger nearby units, thus generating an image classification that more closely matches the homogenous polygons mapped by field teams (e.g., Goovaerts, 2002; Maruca and Jacquez, 2002).

The approach taken in this study was ‘‘top-down,’’ meaning that spectra from the airborne image were used to drive the classification. These image spectra, however, represent a mixture of all the factors affecting the electromagnetic radiation as it travels from the target to the sensor. The reflectance spectra for in-stream habitats, for example, represent variations in reflectance because of surface turbulence, substrate size, substrate color and composition, periphyton, turbidity, and depth, not to mention atmospheric effects. The development of deterministic, ‘‘bottom-up’’ models [such as that devised by Lyon and Hutchinson (1995)] could be valuable for developing classification schemes that can be applied across multiple watersheds and multiple images without requiring such extensive ground truth collection efforts. These models would also provide an important explanatory tool for understanding variations in spectral signals in different settings.

Finally, visual examination of the spectral curves and of unsupervised classifications for both Soda Butte Creek and the Lamar River shows that the hyperspectral sensor is capturing far more information about the stream environment than can be conveyed in a simple four-unit classification or a wood/nonwood dichotomy. HSRH-driven unsupervised classifications of the stream environment coupled with subsequent ground investigations might well open our eyes to critical components of the stream system that have previously been overlooked.

7. Summary and conclusions

Overall classification accuracies for in-stream habitats (glides, riffles, pools, and eddy drop zones) ranged from 69% for third-order streams to 86% for fifth-order streams (Table 2). R^2 values for comparisons of measured and estimated depths ranged from 20% for high-gradient riffles in third-order reaches to 99% for glides in the fifth-order reach (Table 3). The accuracy of woody debris mapping covered a wide range, depending on the threshold value chosen for the matched filter (Table 4). Visual analysis of image-based maps of in-stream habitats (Fig. 6), depths (Fig. 7), and wood (Fig. 5) all suggests that HSRH imagery generated results that are more accurate and useful than the validation statistics alone seem to suggest.

Given clear water and an unobstructed view of the stream, our results indicate that there is great potential for HSRH mapping and monitoring of streams. In a number of cases, accuracies approached or exceeded the 85% value typically expected for remote sensing mapping. The ability to remotely map and monitor stream channels at spatial scales of 1 m raises exciting prospects for the advancement of stream studies. In particular, HSRH has the potential to enable examination of the pattern, process, and scale so critical to understanding fluvial ecosystems (Walsh et al., 1998) at resolutions previously thought to be obtainable only with localized ground-based monitoring (Muller et al., 1993).

Methodological hurdles remain to be overcome, however, before we can be confident in HSRH-based stream maps. In particular, relative to our study, improved procedures should be used or developed

for georectifying images, removing bidirectional reflectance, assessing accuracy (including the field mapping component), and analyzing the tremendous spatial as well as spectral information in HSRH imagery. These methodological advances need to be coupled with a greater understanding of the spectral characteristics of streams in order to explain classification results and their variation among sites. Only if these studies are undertaken and new working tools developed will the full potential of HSRH mapping of streams be realized.

Acknowledgements

This research was supported by the NASA EOCAP program, Stennis Space Flight Center, Mississippi. William Graham, Joseph Spruce, and Greg Terrie of Stennis Space Flight Center all provided important logistical support and technical advice. Robert Ahl, Kerry Halligan, and Jim Rasmussen collected ground truth data. The senior author wishes to thank Samuel Goward for introducing him to the field of remote sensing and supporting his early research efforts to apply remote sensing technology to watershed measurement and modeling.

References

Aspinall, R.J., 2002. Use of logistic regression for validation of maps of the spatial distribution of vegetation derived from high spatial resolution hyperspectral remotely sensed data. Ecological Modelling. Special Issue on Advances in Generalized Linear/Generalized Additive Modelling: from Species' Distribution to Environmental Management 157 (2–3), 301–312.

Aspinall, R., Marcus, W.A., Boardman, J.W., 2002. Considerations in collecting, processing, and analysing high spatial resolution hyperspectral data for environmental investigations. Journal of Geographical Systems 4 (1), 15–29.

Bisson, P.A., Nielson, J.L., Palmalson, R.A., Grove, L.E., 1982. A system of naming habitat types in small streams, with examples of habitat utilization by salmonids during low stream flow. In: Armantrout, N.B. (Ed.), Acquisition and Utilization of Aquatic Habitat Inventory Information. Proceedings American Fisheries Society, Portland, OR, pp. 62–73.

Boardman, J.W., 1989. Inversion of imaging spectrometry data using singular value decomposition. Proceedings, IGARSS'89, 12th Canadian Symposium on Remote Sensing 4, 2069–2072.

Boardman, J.W., 1993. Automated spectral unmixing of AVIRIS data using convex geometry concepts. Summaries, 4th Jet Propulsion Laboratory Airborne Geoscience Workshop, Jet Propulsion Laboratory Publication 93-26. 14 pp. http://popo.jpl.nasa.gov/docs/workshops/93_docs/4.pdf.

Boardman, J.W., 1999. Precision geocoding of low altitude AVIRIS data: lessons learned in 1998. AVIRIS 1999 Proceedings, Jet Propulsion Laboratory, CA. 6 pp. http://makalu.jpl.nasa.gov/docs/workshops/99_docs/7.pdf.

Boardman, J.W., Kruse, F.A., Green, R.O., 1995. Mapping target signatures via partial unmixing of AVIRIS data. Summaries, Fifth JPL Airborne Earth Science Workshop, Jet Propulsion Laboratory Publication 95-1, pp. 23–26. http://popo.jpl.nasa.gov/docs/workshops/95_docs/7.pdf.

Clark, R.N., Livo, K.E., Kokaly, R.F., 1998. Geometric correction of AVIRIS imagery using on-board navigation and engineering data. AVIRIS 1998 Proceedings, Jet Propulsion Laboratory, CA. 9 pp. http://makalu.jpl.nasa.gov/docs/workshops/98_docs/9.pdf.

Congalton, R.G., Green, K., 1999. Assessing the Accuracy of Remotely Sensed Data: Principles and Practices. Lewis Publishers, New York. 137 pp.

Costa, J.E., Spicer, K.R., Cheng, R.T., Haeni, F.P., Melcher, N.B., Thurman, M.E., Plant, W.J., Keller, W.C., 2000. Measuring stream discharge by non-contact methods: a proof of concept experiment. Geophysical Research Letters 27 (4), 553–556.

Gilvear, D.J., Waters, T.M., Milner, A.M., 1995. Image analysis of aerial photography to quantify changes in channel morphology and instream habitat following placer mining in interior Alaska. Freshwater Biology 34, 389–398.

Goovaerts, P., 2002. Geostatistical incorporation of spatial coordinates into supervised classification of hyperspectral data. Journal of Geographical Systems 4 (1), 99–111.

Hardy, T.B., Anderson, P.C., Neale, M.U., Stevens, D.K., 1994. Application of multispectral videography for the delineation of riverine depths and mesoscale hydraulic features. In: Marston, R., Hasfurther, V. (Eds.), Effects of Human-Induced Change on Hydrologic Systems. Proceedings Annual Water Resources Association, Jackson Hole, WY, pp. 445–454.

Harsanyi, J.C., Chang, C.I., 1994. Hyperspectral image classification and dimensionality reduction: an orthogonal subspace projection approach. IEEE Transactions on Geoscience and Remote Sensing 32, 779–785.

Ladd, S., Marcus, W.A., Cherry, S., 1998. Trace metal segregation within morphologic units. Environmental Geology and Water Sciences 36, 195–206.

Legleiter, C.J., Marcus, W.A., Lawrence, R., 2002. Effects of sensor resolution on mapping in-stream habitats. Photogrammetric Engineering and Remote Sensing 68, 801–807.

Lyon, J.G., Hutchinson, W.S., 1995. Application of a radiometric model for evaluation of water depths and verification of results with airborne scanner data. Photogrammetric Engineering and Remote Sensing 61, 161–166.

Lyon, J.G., Lunetta, R.S., Williams, D.C., 1992. Airborne multispectral scanner data for evaluating bottom sediment types and water depths of the St. Marys River, Michigan. Photogrammetric Engineering and Remote Sensing 58, 951–956.

Marcus, W.A., 2002. Mapping of stream microhabitats with high spatial resolution hyperspectral imagery. Journal of Geographical Systems 4 (1), 113–126.

Marcus, W.A., Meyer, G.A., Nimmo, D.R., 2001. Geomorphic control on long-term persistence of mining impacts, Soda Butte Creek, Yellowstone National Park. Geology 29, 355–358.

Marcus, W.A., Marston, R.A., Colvard Jr., C.R., Gray, R.D., 2002. Mapping the spatial and temporal distributions of large woody debris in rivers of the Greater Yellowstone Ecosystem. U.S.A., Geomorphology 44 (3–4), 323–335.

Maruca, S.L., Jacquez, G.M., 2002. Area-based tests for association between spatial patterns. Journal of Geographical Systems 4 (1), 69–83.

Metesh, J., English, A., Lonn, J., Kendy, E., Parrett, C., 1999. Hydrogeology of the upper Soda Butte Creek basin, Montana. Montana Bureau of Mines and Geology Report of Investigation, vol. 7. 66 pp.

Meyer, G.A., 2001. Recent large-magnitude floods and their impact on valley-floor environments of northeastern Yellowstone. Geomorphology 40 (3–4), 271–290.

Minshall, G.W., Robinson, C.T., Robinson, T.V., Royer, T.V., 1998. Stream ecosystem responses to the 1988 wildfires. Yellowstone Science 6 (3), 15–22.

Montgomery, D.R., Buffington, J.M., 1997. Channel-reach morphology in mountain drainage basins. Geological Society of American Bulletin 109 (5), 596–611.

Muller, E., Decamps, H., Dobson, M.K., 1993. Contribution of space remote sensing to river studies. Freshwater Biology 29, 301–312.

Orth, D.J., Maughan, O.E., 1983. Microhabitat preferences of benthic fauna in a woodland stream. Hydrobiologica 106, 157–168.

Richards, J.A., 1994. Remote Sensing Digital Image Analysis. Springer, Berlin. 340 pp.

Spicer, K.R., Costa, J.E., Placzek, G., 1997. Measuring flood discharge in unstable stream channels using ground penetrating radar. Geology 25 (5), 423–426.

Ustin, S.L., Costick, L., 2000. Multispectral remote sensing over semi-arid landscapes for resource management. In: Hill, M.J., Aspinall, R.J. (Eds.), Spatial Information for Land Use Management. Gordon and Breach, London, pp. 97–109. Chapter 8.

Walsh, S.J., Butler, D., Malanson, G.P., 1998. An overview of scale, pattern, process relationships in geomorphology: a remote sensing and GIS perspective. Geomorphology 21, 183–205.

Winterbottom, S.J., Gilvear, D.J., 1997. Quantification of channel-bed morphology in gravel-bed rivers using airborne multispectral imagery and aerial photography. Regulated Rivers: Research and Management 13, 489–499.

Wright, A., Marcus, W.A., Aspinall, R.J., 2000. Applications and limitations of using multispectral digital imagery to map geomorphic stream units in a lower order stream. Geomorphology 33 (1–2), 107–120.